Engineering Fracture Mechanics 266 (2022) 108394

Contents lists available at ScienceDirect

Engineering Fracture Mechanics

journal homepage: www.elsevier.com/locate/engfracmech

Leak before break fracture assessment of pressurized unplasticized PVC pipes with axial surface crack: Experimental and analytical analysis

Mohamed El-Sayed [a], Aly El Domiaty [a], Abdel-Hamid I. Mourad [b,c,d,*], Dinu Thomas Thekkuden [b]

[a] *Mechanical Engineering Department, Suez Canal University, Ismailia, Egypt*
[b] *Mechanical and Aerospace Engineering Department, College of Engineering, United Arab Emirates University, Al-Ain, P.O. Box. 15551, United Arab Emirates*
[c] *On Leave from Mechanical Design Department, Faculty of Engineering, El Mataria, Helwan University, Cairo, Egypt*
[d] *National Water and Energy Center, United Arab Emirates University, Al-Ain, P.O. Box. 15551, United Arab Emirates*

A R T I C L E I N F O

Keywords:
Leak Before Break
Failure Assessment Diagram
Burst Pressure
Stress Intensity Factor
Polymeric Material

A B S T R A C T

This paper compares Failure Assessment Diagram-based and Stress Intensity Factor-based analytical approaches with experimental results for assessing leak before break in axial finite semi-elliptical cracked Polyvinyl Chloride pipes subjected to internal pressure. Surface crack length of 25, 40 and 60 mm and depth to thickness ratio of 0.25, 0.5 and 0.75 were investigated. Burst pressures are experimentally evaluated for all cracked and uncracked samples. Results illustrated that the Failure Assessment Diagram approach is more reliable than Stress Intensity Factor approach for fracture assessment of unplasticized PVC pipes.

1. Introduction

The leak-before-break (LBB) is a concept producing the leak before the complete collapse of part-through cracked components after propagating to a stable through-thickness crack by the action of internal pressure. The LBB behavior provides sufficient warning about the near-collapse of pressurized components. In this regard, LBB is considered a safety measure and an important requirement for the safety of the design. Due to these reasons, LBB methodologies have drawn the attention of various researchers for implementing in different applications such as nuclear piping, gas and oil pipelines, and pressure vessels, etc. Exposure to the failure mechanisms can promote the generation of crack tips and stable crack growth [1,2]. Kawaguchi et al. [3] have examined the LBB behavior for axially notched X65 and X80 gas pipelines. Kim [4] has performed LBB analysis on through-thickness cracked pipes. Kim et al. [5] have proposed an elastic–plastic J-integral approach to perform the LBB analysis for circumferential through-thickness cracked pipes. Sharples [6] stated that all the LBB procedures shared the same basis of specifying the flaw size. El-Sayed et al. [7] summarized the LBB procedure used in assessing the integrity of cracked pipeline in a simple flowchart and studied the possibility of forming stable through-thickness cracks in pipelines made of X70 steel during service under internal pressure. There are several instances of defects embedded in the components without being noticed even after the quality inspection checks. The cracks of different forms propagate

* Corresponding author at: Mechanical and Aerospace Engineering Department, College of Engineering, United Arab Emirates University, Al-Ain, P.O. Box. 15551, United Arab Emirates.
E-mail address: ahmourad@uaeu.ac.ae (A.-H. I. Mourad).

https://doi.org/10.1016/j.engfracmech.2022.108394
Received 23 July 2021; Received in revised form 14 February 2022; Accepted 16 March 2022
Available online 21 March 2022

Nomenclature

Symbols

a	Crack Depth
c	Half Crack Length
D	Pipe Outer Diameter
R_o	Outer Radius
R_i	Inner Radius
R_m	Mean Radius
t	Pipe Wall Thickness
b	Width of Tensile Test piece
E	Young's Modulus
α	Curve Fitting Parameter
n	Strain Hardening Exponent
K_I	Stress Intensity Factor
K_{Ic}	Plane Strain Fracture Toughness Characterized by K-factor
K_{app}	Applied Stress Intensity Factor
M	Magnification Factor
C_f	Correction Factor of Curvature of A Cylindrical Shell
$E_{(k)}$	Crack Shape Factor
P	Internal Pressure
P_B	Burst Pressure
P_r	Actual Burst Pressure in radial direction
P_{app}	Applied Normal Burst Pressure
F_{max}	Maximum Applied Force
μ	Friction Coefficient
$d_i^{'}$	Inner Diameter at Maximum Bulging of the pipe
σ_φ	Hoop Stress
σ_{app}	Applied Stress
σ_f	Flow Stress
σ_o, σ_y	Yield Strength
σ_{ult}	Ultimate Tensile Strength
σ_m	Membrane Stress
ε_o, ε_y	Yield Strain
K_r	Toughness Ratio
L_r	Load Ratio
L_r^{max}	Localized Plastic Collapse Limit

Abbreviations

PVC	Polyvinyl Chloride
UPVC	Unplasticized Polyvinyl Chloride
FAD	Failure Assessment Diagram
SDR	Standard dimension ratio
SIF	Stress Intensity Factor
SB-FAD	Stress Based Failure Assessment Diagram
LBB	Leak Before Break
LEFM	Linear Elastic Fracture Mechanics

by one or more failure mechanisms accelerating the damage. Mode I, mode II, mode III and mixed mode crack propagation are widely common in the presence of surface cracks [8–16]. These cracks on the external or internal surfaces of in-service pipes, tanks, or other industrial systems ultimately diminish the integrity of the material consequently reducing the service life of the systems [17,18].

The majority of the studies discussing the LBB have focussed on the material defects and geometrical imperfections in metallic pipes using experimental, analytical and numerical techniques of the fracture assessment. Based on these studies, a multitude of assessment methods that are dealing with the effect of the defect geometry and material type on pipe's structural integrity is available in the literature [7,19–27]. However, studies focussing on the failure of pipes made of polymeric material are very rare, e. g., using a semi-empirical model [28]. Other researches were more oriented towards studying the effects of ageing and chemical degradation on the durability and service life of a polymeric pipe [29–31]. There are various types of polymeric pipes classified according to their nature of use and chemical composition such as Cross-linked Polyethylene (PEX), Polyvinyl Chloride (PVC), Unplasticized Polyvinyl Chloride (uPVC), Acrylonitrile Butadiene Styrene (ABS), and High-density Polyethylene (HDPE). In the general case, polymeric pipelines are used across the globe for applications such as water, gas and sewer facilities, slurry transfer lines, rural irrigation, fire system supply lines, electrical and communications conduit, and storm water and drainage pipes. The polymeric pipes have excellent properties such as high corrosion and chemical resistance, low cost, flexibility, durability, and ease of installation [32]. Therefore, polymeric pipes have a wide scope for various applications. However, any presence of surface defects that are generated during the installation or maintenance operations or by other external factors such as the incorrect use of a cutting tool affect the maximum/failure pressure of the pipe [28]. Under certain load conditions during service or the effect of overpressures caused by the transient flow [33], these faults may increase and gradually shorten the remaining service life or cause catastrophic failure. By using the fracture mechanics, it is possible to evaluate the threat of such defects to carry out the proper countermeasures. Although surface defects can occur in various directions, El-Sayed et al. [19] investigated the longitudinal semi-elliptical cracks that have been subjected to the highest hoop stress in the pipe wall [34]. In another work by El-Sayed et al. [7], it has been illustrated that the propagation of a semi-elliptical crack is initiated from the deepest point, and is oriented in the radial direction rather than longitudinal direction on the external surface of the pipe. The results of different assessment methods for axial surface crack in steel pipes subjected to internal pressure proved that the assessment method that gives smaller critical crack size is more conservative compared to larger cracked sizes. In addition, a simplified LBB approach for periodical assessments of crack length ($2c$), as well as crack depth (a) to control the risk of rupture, has been formulated. The harmfulness of the presence of longitudinal semi-elliptic cracks in a polymeric pipe has been evaluated by determining the J-integral using a semi-empirical model [35]. The numerical Finite Element FE model is used previously to study the defect size influence on the toughness and the crack initiation pressure as well as the countermeasures such as stffners and bandages to prevent crack propagation [34,36]. The numerical FE model results of a pre-cracked pipe are verified and compared with the experimental results [37,38]. Guidara et al. [37] conducted a study on the structure integrity assessment of defected high density poly-ethylene pipe using burst test and finite element analysis FEA based on J-integral criterion. The results proved that the numerical analysis is in a good agreement with the experimental burst test. Similarly, Guidara et al. [38] analyzed HDPE pipe failure under overpressure in presence of a longitudinal surface defect and illustrated that the material behaviour has been correctly applied to the model, burst tests were reproduced numerically and experimentally with the aim to calculate the crack initiation pressure under the same test conditions (loading rate, pipe size, crack geometry, boundary conditions).

On the other hand, an ultrasonic non-destructive inspection technology for the assessment of plastic pipes under grooves and cracks, provide a measure of the structural integrity of the pipe, as well as 'looking' through the pipe wall to assess the void formation and critical loss of support [39,40]. Ghazali et al. [39] have used the ultrasonic guided wave method to detect cracks in a plastic pipe and the experimental results suggested using the technique for enhancing the validity and precision of pipeline crack detection in uncracked and cracked pipe. Zhu et al. [40] have conducted a non-destructive in-situ condition assessment of plastic pipe using ultrasound and reported that the technique is a comprehensive diagnostic tool for plastic pipe inspection having the capability to be used in assessing the integrity of buried pipelines under a wide range of soil particle sizes. In the manufacturing stage, the structural integrity of the pipes is estimated by evaluating the burst pressures. The burst pressure indicates the maximum pressure that the pipe can withstand before rupturing under the action of internal forces. In addition, the burst pressure tests in accordance with several international standards are used to determine the failure mode and factor of safety. It is mandatory for the working pressure to be within the burst pressure for safe operation. International standards such as ISO 1167, ASTM D 1598–21, ASTM D 1599, ISO 9080, CJ/T 108, ASTM F1335 are followed in industries to determine the resistance to internal hydrostatic pressure of the unnotched pipes by conducting the burst tests. Pipes burst out in the presence of cracks under the action on working pressure. Therefore, pipe manufacturers follow certain international standards for determining the slow crack propagation. ISO 13479 and ISO 16241 standards prescribe the resistance to the crack propagation in a notched polyolefin pipes and notched polyethylene pipes respectively. ISO/TS 16479 based on notched ring test determines the slow crack resistance of thermoplastic pipes. Standard procedures for the preparation of notches for evaluating fracture toughness of uPVC and modified PVC using C rings are prescribed in ABNT NBR 7665, PAS 27, AS/NZS 4765 and SANS 966–2 [41]. Even though the current paper focusses on exerting an internal pressure using steel balls, hydrostatic pressure using standard hydrostatic pressure tester is performed by the manufacturers to quantify the burst pressure conforming to above mentioned standards [42,43]. The proposed approach requires validation of the burst pressure for different cracked pipe conditions in future with the hydrostatic pressurizing method.

Nowadays, steel pipes are replaced with uPVC pipes for certain applications. However, the uPVC pipes and other plastics under certain conditions can fail in a brittle mode [44]. Consequently, the brittle fracture of uPVC has received increasing attention from many researchers. Many brittle fracture techniques have been adopted from metals technology [45]. The metal structural materials deform plastically above their yield stress, in reality, it is well known that due to the stress concentration at the crack tip, even the most brittle failures involve some plastic deformation near the crack tip. The theoretical basis of most brittle fracture studies is linear elastic fracture mechanics (LEFM). The concepts of LEFM were successfully applied to characterize the fracture behavior of thin uPVC pipes at high loading rate similar to those applied for metals [45,46]. However, there is no clear theoretical assessment method to characterize semi-elliptical surface crack in PVC pipes. This reality has provided the motivation for the present study.

In the light of the above review, articles focusing on the defected polymeric pipes are rare. A new technique for evaluating the leak before break phenomenon by exerting an internal pressure in the defected pipes using steel balls is proposed. The main objective of the present work is to evaluate experimental and analytical analyses on pressurized uPVC pipes for assessing the impact of the presence of longitudinal surface defects on the pipe wall.

2. Materials

The uPVC pipes used for the experimentation were provided by Al-Amal Company at the 10th of Ramadan, Egypt. The uPVC pipes were according to ASTM D 2241 (SDR Series) standard having a nominal pressure of 1.1 MPa. The SDR 26 category uPVC pipes with working pressure limited to 1.1 MPa is used for the research. The burst pressure of the pipe is 2.4 MPa according to the manufacturer. The pipes having an outer diameter of 110 mm, a wall thickness of 4 mm and a length of 6000 mm were cut into test coupons with 200 mm length. The pipes are considered thin-walled structures since the (R/t) ratio is greater than 10. An artificial axial finite semi-elliptical surface defect on the surface of uPVC pipes was prepared to represent external cracks using a disc cutter machine having a thickness of 0.5 mm disc thickness. Various sizes with crack lengths (2c) of 25, 40 and 60 mm and depth to thickness ratio (a/t) of 0.25, 0.5 and 0.75 are investigated by artificially creating the cracks. The notch is 'U shaped' notch with tip radius of 0.25 mm (crack width = 0.5 mm). Fig. 1 illustrates the geometry of the pipes and details of the crack and notch.

3. Theoretical analysis of an axial crack in a pipe

3.1. SIF of longitudinal semi-elliptical surface crack

Many researchers have proposed different methods to estimate the stress intensity factor (SIF) for longitudinal semi-elliptical surface crack in cylindrical pipe walls (Fig. 1), such as finite element method, boundary integral equations method and other alternative methods (e.g, the weight function method). The solutions for an elliptical plane crack in an infinite 3D body were used to derive the solutions for semi-elliptical surface cracks found in a plate subjected to uniaxial tension [47]. The solution was then adjusted by Shah and Kobayashi [48] by introducing correction factors for the front and rear surface of the pipe and for the plastic region at the crack tip to account for the finite thickness of the pipe as well as the plastic zone at the tip of the crack. Due to the disagreements shown by various solutions, Scott and Thorpe [49] tested these solutions accuracy and concluded that Newman's solution [50] provides the best SIF prediction for a part-through crack in a plate. The solution was then adjusted for a thin-wall cylinder under internal pressure containing an axial surface crack as given by Eq. (1).

$$K_I = \frac{\sigma_\varphi \sqrt{\pi a}}{E_{(k)}} M \tag{1}$$

where,
a is the crack depth
Hoop stress $\sigma_\varphi = \frac{PR_m}{t}$
P is the internal pressure
R_m is the mean radius of the pipe wall
t is the wall thickness of the pipe
M is magnification factor ($M = C_f\, M_e$)

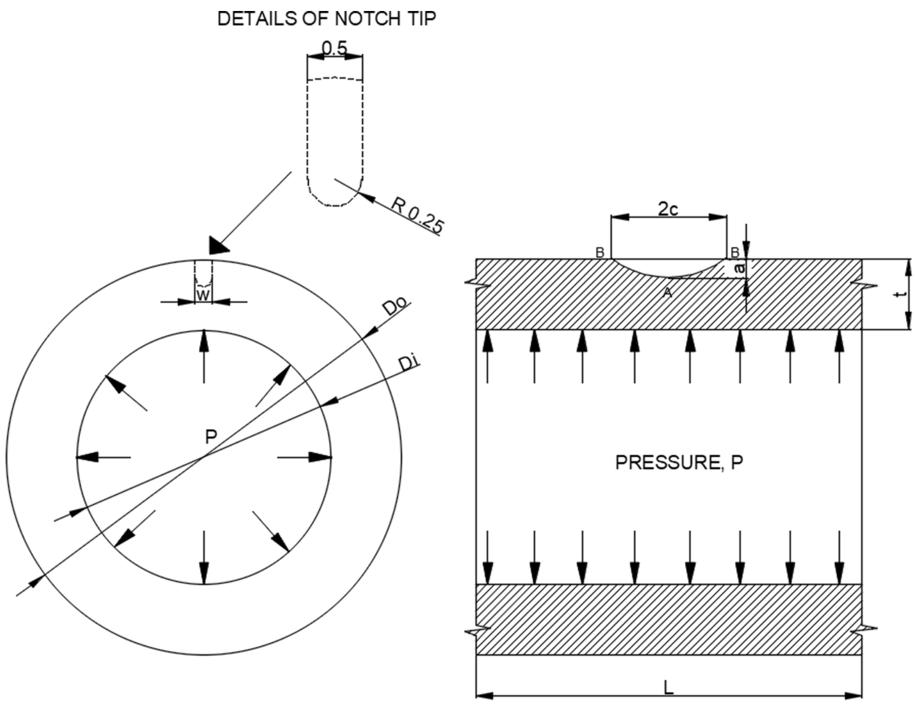

Fig. 1. Geometry of a pipe subjected to an internal pressure with an external axial semi-elliptical surface crack.

C_f is the correction factor for the curvature of a cylindrical shell [20]

$$C_f = \frac{\left(1 - \frac{a/t}{\sqrt{1+1.255\left(c/\sqrt{R_m t}\right)^2 - 0.0135\left(c/\sqrt{R_m t}\right)^4}}\right)}{(1 - a/t)}$$

$$M_e = M_F + \left(E_{(k)}\sqrt{c/a} - M_F\right)\left(\frac{a}{t}\right)^s$$

c is the half of the surface crack length

M_F and s are functions depending on the crack geometry (a/c ratio) and the relative crack depth (a/t ratio). These functions differ in their form for the lowest point of the crack tip (Point A in Fig. 1) and for the crack mouth on the surface of the cylindrical shell (Point B in Fig. 1).

$$M_F = 1.13 - 0.1\left(\frac{a}{c}\right) \quad \text{for } a \leqslant c$$

$$M_F = \sqrt{\frac{c}{a}}\left[1 + 0.03\left(\frac{c}{a}\right)\right] \quad \text{for } a > \text{c}$$

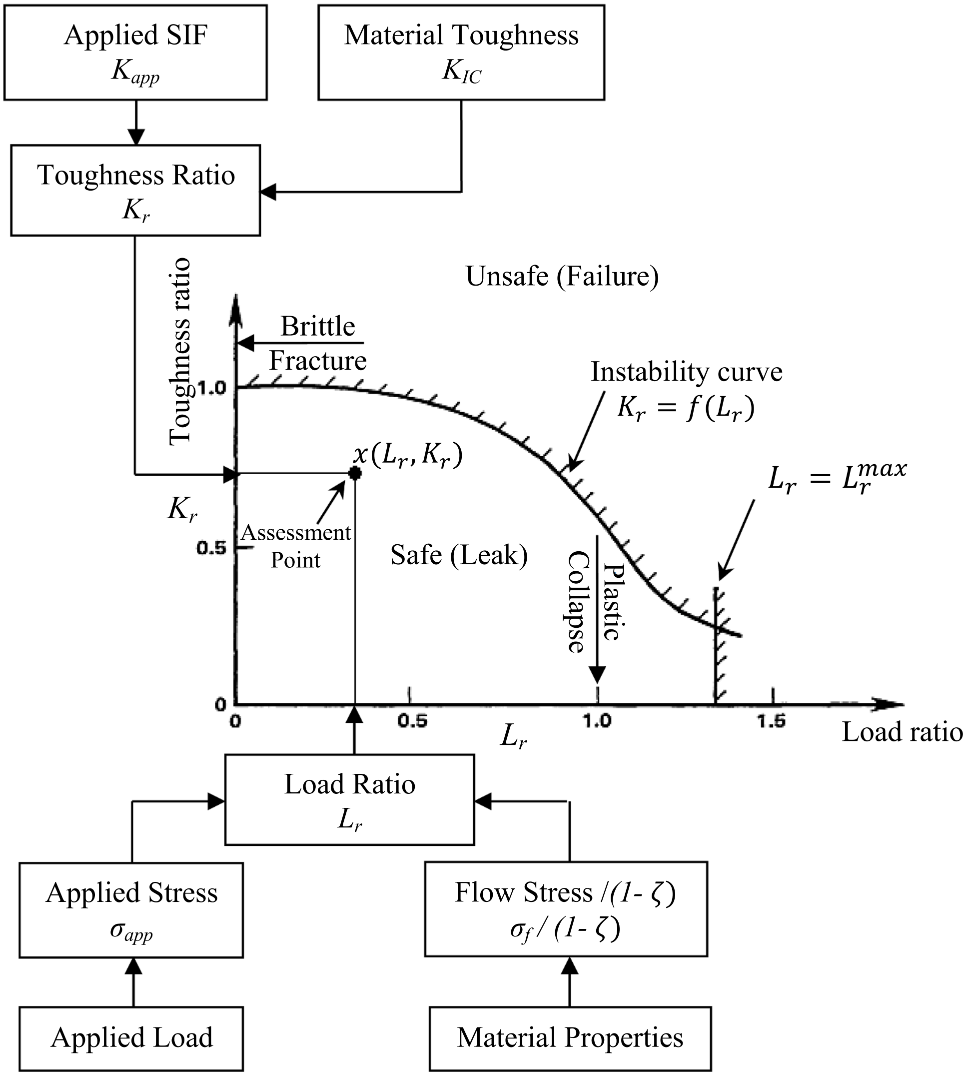

Fig. 2. Failure Assessment Diagram generation procedure and assessment criteria.

$$s = 2 + 8\left(\frac{a}{c}\right)^3 \quad \text{for } a \leqslant c$$

Crack shape factor $E_{(k)}$.

$$E_{(k)} = 1 + 1.464\left(\frac{a}{c}\right)^{1.65} \quad \text{for } a \leqslant c$$

$$E_{(k)} = 1 + 1.464\left(\frac{c}{a}\right)^{1.65} \quad \text{for } a > \text{c}$$

3.2. Stress based failure assessment diagram

The failure assessment diagram (FAD) is a graphical representation of two parameter failure criterions such as unstable fracture criterion and plastic collapse criterion. FAD is applied mainly for the assessment of crack-like flaws. R6 procedure [51,52] is widely known for generating the failure assessment diagram. To construct this diagram, it is necessary to calculate two parameters, namely, non-dimensional crack driving force K_r and non-dimensional applied stress ratio L_r as shown in Fig. 2. The toughness ratio K_r represents the probability of a structure to undergo brittle fracture. It is calculated from Eq. (2) by dividing the fracture mechanics parameter (stress intensity factor SIF) obtained analytically over the material fracture toughness (K_{Ic}) determined from the fracture toughness standard test [53,54]. Load ratio (L_r) represents the probability of a structure to undergo plastic collapse. The load ratio is evaluated using the Eq. (3) from the stress intensity factor and limit load handbook [55]. These equations are limited to crack depth to wall thickness ratio less than 0.8 and the investigated range, 0.25 to 0.75, in this experimentation falls within 0.8.

$$K_r = \frac{K_{app}}{K_{Ic}} \tag{2}$$

$$L_r = \frac{g(\zeta)\frac{\sigma_b}{3} + \sqrt{g^2(\zeta)\frac{\sigma_b^2}{9} + (1-\zeta)^2\sigma_m^2}}{(1-\zeta)^2\sigma_y} \tag{3}$$

where,

$$\sigma_m = \sigma_{app} = \sigma_{hoop} = \frac{P.R_m}{t}$$

$$\sigma_b = 0$$

$$\zeta = \frac{al}{t(l+2t)}$$

σ_y is the yield stress
σ_m is the membrane stress
a is the crack depth
l is the length of the crack
t is the thickness of pipe

The relationship between K_r and L_r defines the instability curve of the failure assessment diagram. The instability curve separates the safe (leak) and unsafe (failure) regions. This curve in terms of non-dimensional load is given by equation Eq. (4) [22,51].

$$f(L_r) = \left(1 - 0.14L_r^2\right).\left(0.3 + 0.7\exp\left(-0.65L_r^2\right)\right) 0 \le L_r \le L_r^{max} \tag{4}$$

and the cut-off ratio is defined using Eq. (5) [22,51].

$$L_r^{max} = \frac{1}{2}\left(1 + \frac{\sigma_{ult}}{\sigma_y}\right) \tag{5}$$

The assessment point is obtained by using the toughness and load ratios as given by Eq. (2) and Eq. (3), respectively, and then drawn on the FAD. The critical assessment points which indicate fracture instants, form an assessment instability curve limited between two reference states namely, brittle fracture state [$K_r = 1$ and $L_r = 0$] and plastic collapse state [$K_r = 0$ and $L_r = 1$]. The assessment point of a structure can be determined by plotting a point of coordinates K_r and L_r. If the assessment point falls inside the instability curve, then the structure is considered safe against brittle and plastic failures. However, if the assessment point falls outside the instability curve, then the structure would fail by brittle fracture (unstable crack growth) or another possible failure is due to exceedance of the limit load, namely, plastic collapse as illustrated in Fig. 2.

4. Experimental work

4.1. Tensile test

Since most failure prediction methods are stress-based, accurate material properties are required for accurate prediction of the failure pressure. The material properties were determined with uniaxial tensile tests of samples oriented to the longitudinal direction of the pipe according to ISO 6259–3:1997 [56]. However, ISO 6259–2: 2020 is more preferable for estimating the stress–strain characteristics of uPVC pipes. Four tensile samples are cut equally from the wall of the pipe and the sample dimensions are shown in Fig. 3. It has a thickness equal to the wall thickness of the pipe (4 mm) and a width of 10 mm. The uniaxial tensile test in the longitudinal direction is carried out using a universal testing machine. Fig. 4 shows the tensile sample before, while and after testing. The samples were tested at a moving clamp velocity of 5 mm/min. It was observed that the sample fractured without considerable deformation and necking. The fracture plane occurred at almost a perpendicular direction to the applied loading.

4.2. Burst test

Samples for the burst test were fabricated using the same procedures. Fig. 5 shows the tools used for preparing the specimens for burst testing. The cylindrical test specimens were cut with the same original dimensions of the uPVC pipe (length of 200 mm, outer diameter of 110 mm, and thickness of 4 mm). Then the location of the artificial defect for each test specimen has been determined. A disc cutting machine and a round file were used to make an axial surface crack with various sizes in the wall of the test specimens as shown in Fig. 5. Vernier caliper was used to measure the dimensions of the test specimens and the artificial defects. Three different crack lengths, $2c = 25$, 40 and 60 mm and the depth to thickness ratio, $a/t = 0.25$, 0.5 and 0.75 were considered. Therefore 10 different groups with three identical samples each were prepared. Hence, the total number of specimens is 30 including the specimens without crack. A dial indicator was used to measure the radial bulging deformation during and after the burst test.

Fig. 6 depicts an overall photograph of the prepared test specimens before the burst testing. Fig. 7 shows represented photographs of the setup for specimens with artificial crack length $2c$ of 40 and 60 mm and crack depth 2 and 3 mm.

Two steel cylindrical blocks of 100 mm diameter and 100 mm length were installed into the bottom and the top ends of the test specimen. The specimen was filled with spherical steel balls (of ball bearing) of 10 mm diameter between the two blocks to a height of 50 mm as shown in Fig. 8. These specimens were pressurized by compressing the two blocks between the two plates of the universal testing machine to determine the maximum force that each specimen can withstand till failure. Some of the fractured specimens are shown in Fig. 9. The compression force increased by applying an overhead speed of 5 mm/min. The maximum/failure compression force is the force at which the artificial defect starts to grow till a through crack is formed. Then the spherical balls were pushed out of the pipe and the failure occurred as in leak before break phenomena. It was observed that the crack starts to propagate at its deepest point in the radial direction and also propagates simultaneously in the longitudinal direction. It is worth mentioning that the specimens were suddenly broken at a certain length and depth of the crack during some tests before the leakage indicating break before leak. The stopping criterion was based on the clear drop in the applied load. In the case of small crack lengths, the applied load increased even after the balls came out and at a certain point after some balls dropped out (Leak before break), the applied load decreased. But in some large cracks, the load decreased after the first ball came out from the pipes indicating fracture before leak. Preliminary experiments were carried out with sand and marbles expecting a lateral force being exerted on the pipe walls under the action of compressive force. For the case of sand, the sand has initial compactness which limited more compactness to take place. Thus, the lateral radial force on the wall was very small to the extent that the explosion has not been taken place. For the case of marbles, the problem was that some of the marbles were crushed while applying the axial compression force and the lateral radial force on the wall of the pipe got affected significantly. However, an alternate choice of steel balls replacing the sand and marbles has been successful to distinguish leak before break and break before leak for various investigated crack dimensions.

Fig. 10 shows the test specimens after burst testing and the associated bulging due to the internal pressure. The failure for each test specimen for the different crack sizes is presented in Table 1. The crack propagation initiation location was determined based on the deepest point in the artificial defect profile. The crack propagation is followed by the bulging of the pipe wall, necking through the wall thickness, and finally the specimen failure. The bulging area is affected by the crack size and reached its maximum value for the uncracked specimen. During continued growth, the necking appeared and penetrated deeper towards the pipe interior. For those pipes with crack lengths 25 mm and 40 mm at different crack depths, crack propagated and developed through thickness-crack before the collapse of the pipes causing leak before break. But in the specimen with 60 mm length having 2 mm depth, the crack has propagated

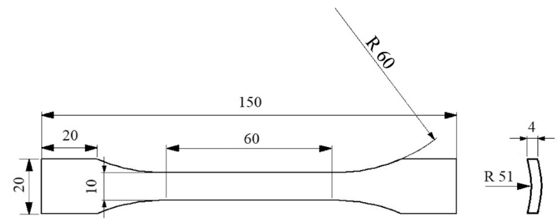

Fig. 3. Tensile test sample. All dimensions are in mm.

Fig. 4. The tensile sample before, while and after testing.

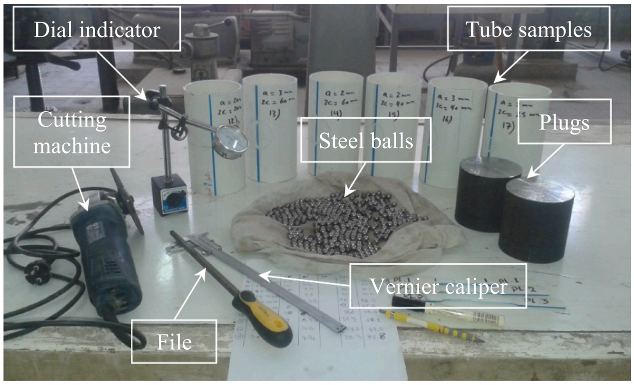

Fig. 5. Tools used for preparing specimens for burst testing.

Fig. 6. Test specimens that were prepared for the burst test.

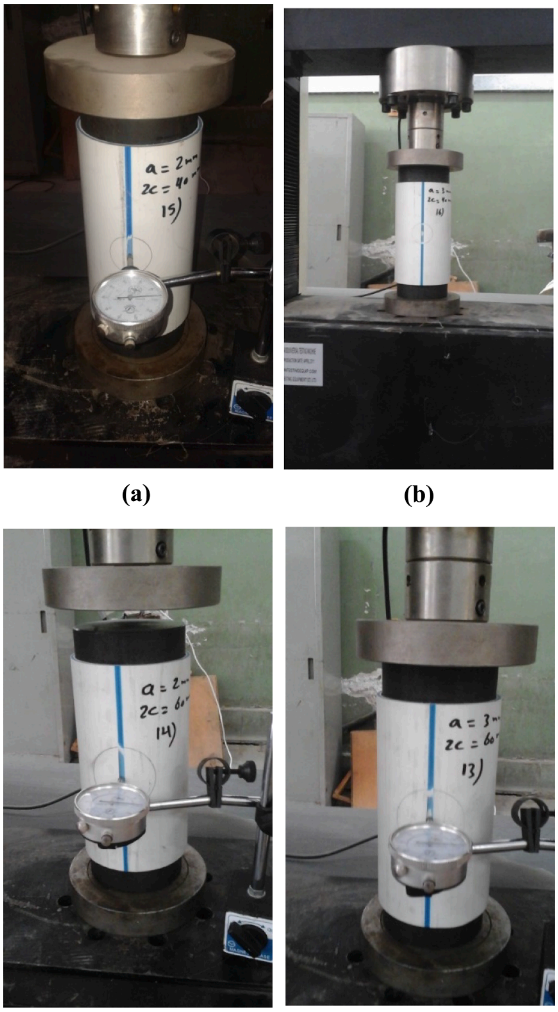

Fig. 7. Setup of the burst test of test specimens. Crack length $2c = 40$ mm (depth $a =$ (a) 2 mm and (b) 3 mm) and crack length $2c = 60$ mm (depth $a =$ (c) 2 mm and (d) 3 mm).

creating shear lips near the pipe surfaces and causing sudden failure prior to leakage (Break before Leak). The range of crack lengths and crack depths used for the experimentation are able to clearly distinguish leak before break and break before leak phenomenon.

5. Results and discussion

5.1. Experimental results

5.1.1. Tensile test results

The engineering and true stress–strain curves for the tensile test are shown in Fig. 11 and Fig. 12, respectively. The true strain and stress are calculated from Eqs. (6) and (7), respectively, where the volume is constant. The constancy of volume is only valid up to the point of necking where the deformation becomes localized in the tensile specimen. Both the engineering stress–strain and true stress–strain curves are nearly identical with coinciding yield strength and elastic modulus.

$$\varepsilon_{True} = ln\left(1 + \varepsilon_{Eng}\right) \tag{6}$$

$$\sigma_{True} = \sigma_{Eng}\left(1 + \varepsilon_{Eng}\right) \tag{7}$$

The Ramberg-Osgood equation expresses the total strain as the sum of the elastic and plastic strain in terms of three parameters (i.e., α, n and σ_y). This is useful since it provides a simple way of describing the true material behavior as presented by Eq. (8).

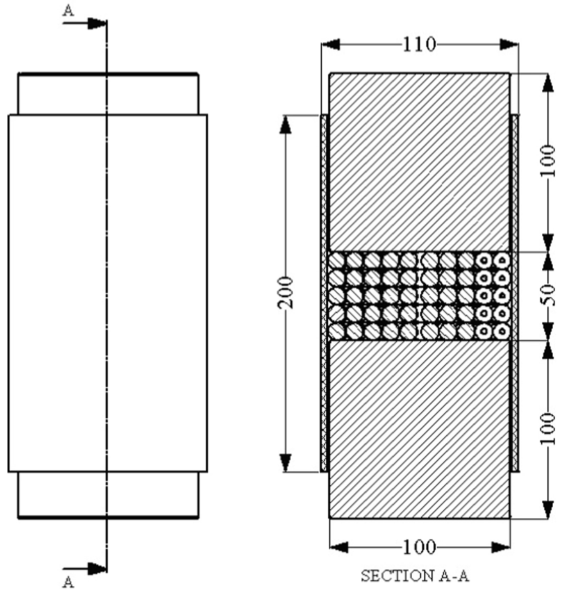

Fig. 8. A schematic drawing of the specimen (with the two blocks) prepared for burst test. All dimensions are in mm.

Fig. 9. Failure of cracked specimens in the burst test.

Fig. 10. Specimens after burst testing.

$$\frac{\varepsilon}{\varepsilon_o} = \frac{\sigma}{\sigma_o} + \alpha\left(\frac{\sigma}{\sigma_o}\right)^n$$

$$\varepsilon_{Total} = \varepsilon_{Elastic} + \varepsilon_{Plastic}$$

$$\varepsilon_{Total} = \frac{\sigma}{E} + \frac{\alpha}{E}\left(\frac{\sigma}{\sigma_o}\right)^{n-1}\sigma \tag{8}$$

The yield stress was determined from the peak value in the engineering stress–strain curve. The constants α and n were then calculated from a non-linear regression on the true stress–strain tensile test data. It has been found that this equation accurately represents the true stress–strain curve for the tested uPVC material. The results of the tensile test are summarized in Table 2. As listed in Table 2, the experimental laboratory tensile test results are found to be in good agreement with the specifications from the Al-Amal company.

5.1.2. Burst test results

In the burst test, the relationship between the applied load in KN (or the applied pressure) and the overhead displacement in mm was obtained. The load increased with the overhead displacement until it reached the maximum value and beyond. At the maximum load, the crack started to open and propagate. During the propagation of the crack, the force started to decrease with a continuous increase in the displacement until the test was terminated at a specific overhead displacement. The burst pressure of the specimen is obtained by dividing the maximum applied force over the pipe inner area at the maximum bulging which takes place at the mid-span of the pipe length;

$$P_B = \frac{F_{max}}{\frac{\pi}{4}\cdot\left(d_i^{'}\right)^2}$$

where $d_i^{'}$ is the inner diameter at maximum bulging of the pipe.

The actual burst pressure in a radial direction P_r acting perpendicular to the pipe specimen wall is less than the applied normal pressure in an axial direction P_{app} due to the friction coefficient (μ), which can be expressed by the following relation,

$$P_r = P_{app}(1 - \mu)$$

This relationship was first proposed in 1960 by W.M. Long and succeeded by authors [57–59], where the former article provides a fairly satisfactory description of the actual relationship between radial and axial pressure occurring when the metal powder is being compacted in a rigid die. The friction coefficient is usually between zero and one. A value of zero means there is no friction as in the liquid case. A value of unity means that the friction is maximum because the surfaces become very rigid, but it is actually always less than unity [60].

Fig. 13 shows the burst pressures for the tested specimens that contain axial surface defects with a certain length ($2c$) and depth (a) by using an assumed friction coefficient of 0.3 between the steel balls with the pipe wall. The coefficient of friction between the metal and plastics lies in the range of 0.25 to 0.4 [61]. The friction coefficient between the steel balls bearing with each other in the presence of a gasoline lubricant is neglected because of the very small value. The average burst radial pressure of the three uPVC pipes is estimated experimentally to be 2.37 MPa. Fig. 13 shows the burst pressures of cracked specimens for the various cases of crack

Table 1
Test specimen with crack length (2*c*) mm and depth (*a*) mm.

Crack size, mm		Depth, *a*		
		1	2	3
Length, 2*c*	25	 Leak before break	 Leak before break	 Leak before break
	40	 Leak before break	 Leak before break	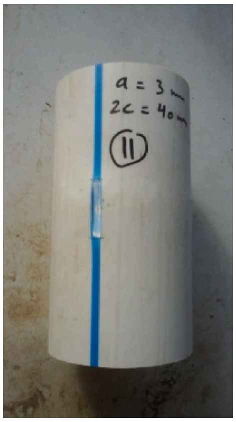 Leak before break
	60	 Leak before break	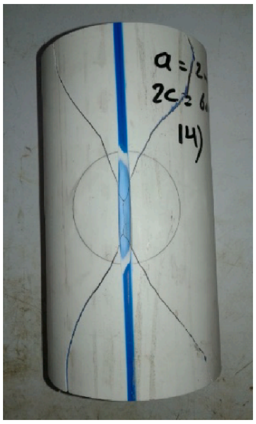 Break before leak	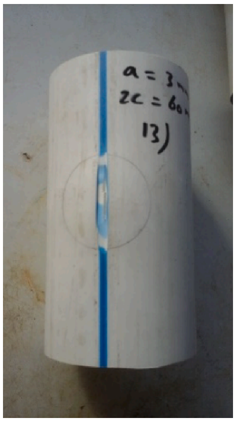 Leak before break

dimensions. It is evaluated that the burst pressure decreased with the increase in the critical depth to thickness ratio for each of the fixed crack lengths. The percentage reductions of burst pressure in the absence of a crack to each case of varying crack length 25 mm, 40 mm and 60 mm at a certain ratio $(a/t) = 0.25$ are 16.45 %, 21.94 % and 26.58 %, respectively. Similarly, the percentage reductions of burst pressure at $(a/t) = 0.5$ are 19.8 %, 26.16 % and 30.8 % respectively whereas the percentage reductions of burst pressure at $(a/t) = 0.75$ are 24.4%, 32.1% and 39.24% respectively for the crack lengths of 25 mm, 40 mm and 60 mm. Also, the burst pressure was found to decrease with the increase in the crack length. It is worth mentioning that the burst pressure at 60 mm crack length was the

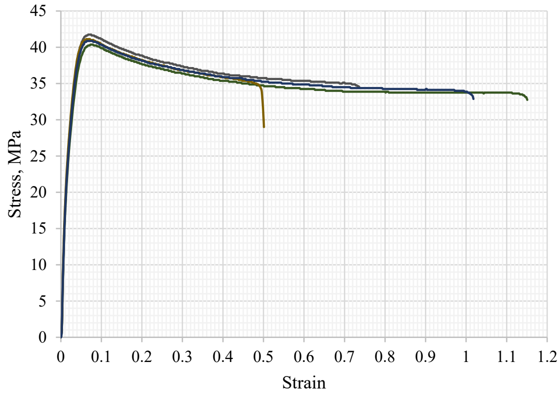

Fig. 11. Engineering stress–strain curves for a uPVC material.

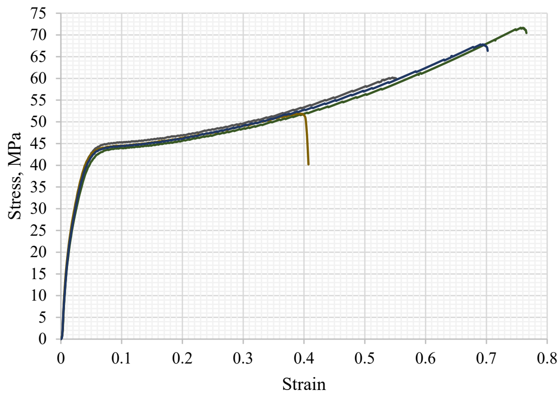

Fig. 12. The True stress–strain curves for a uPVC material.

Table 2
The properties of a uPVC material (white powder) used.

Source			Testing Laboratory	Al-Amal Company
D		(mm)	110	110
b		(mm)	10	6.34
t		(mm)	4	4
$\sigma_y = \sigma_u$	*Mean*	(MPa)	41.03	40
	Std. Dev	(MPa)	0.317	–
ε_y	*Mean*	%	7	6.68
	Std. Dev	%	0.408	–
E	*Mean*	(MPa)	653.2	652.8
	Std. Dev	(MPa)	29.54	–
α			2.8	–
n			3.06	–
σ_{Break}	*Mean*	(MPa)	32.325	38.7
	Std. Dev	(MPa)	2.342	–
ε_{Break}	*Mean*	%	85.5	70.8
	Std. Dev	%	0.294	–

lowest and the pipes failed catastrophically before leakage indicating the phenomenon break before leak for the specimens with 2 mm depth.

From the experimental data, a relationship between the burst pressure and crack depth to pipe thickness ratios a/t are derived as shown in Fig. 13. The relationships are recommended at the design stage to predict the burst pressure and to find the critical limit that distinguishes leak before break and break before leak.

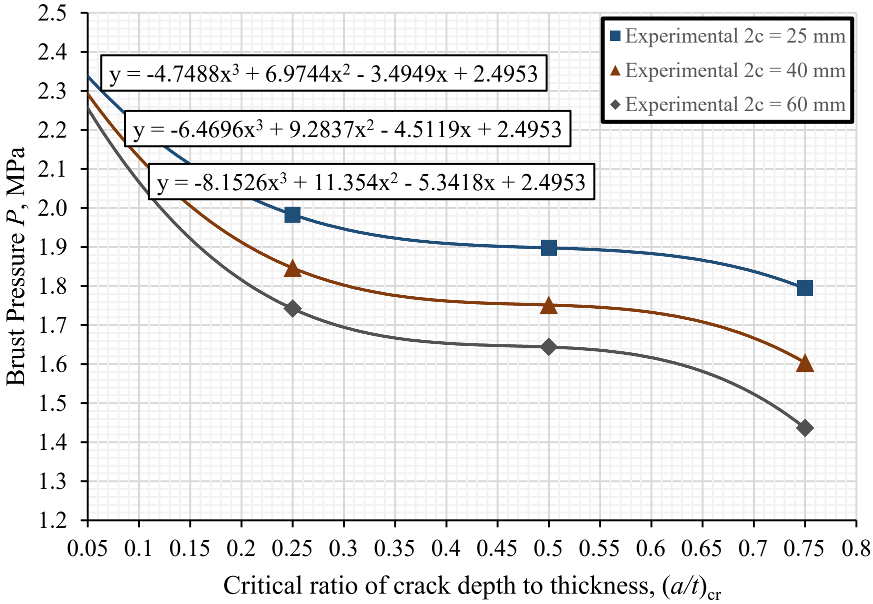

Fig. 13. Variation of the average burst pressure with $(a/t)_{cr}$ for each crack size.

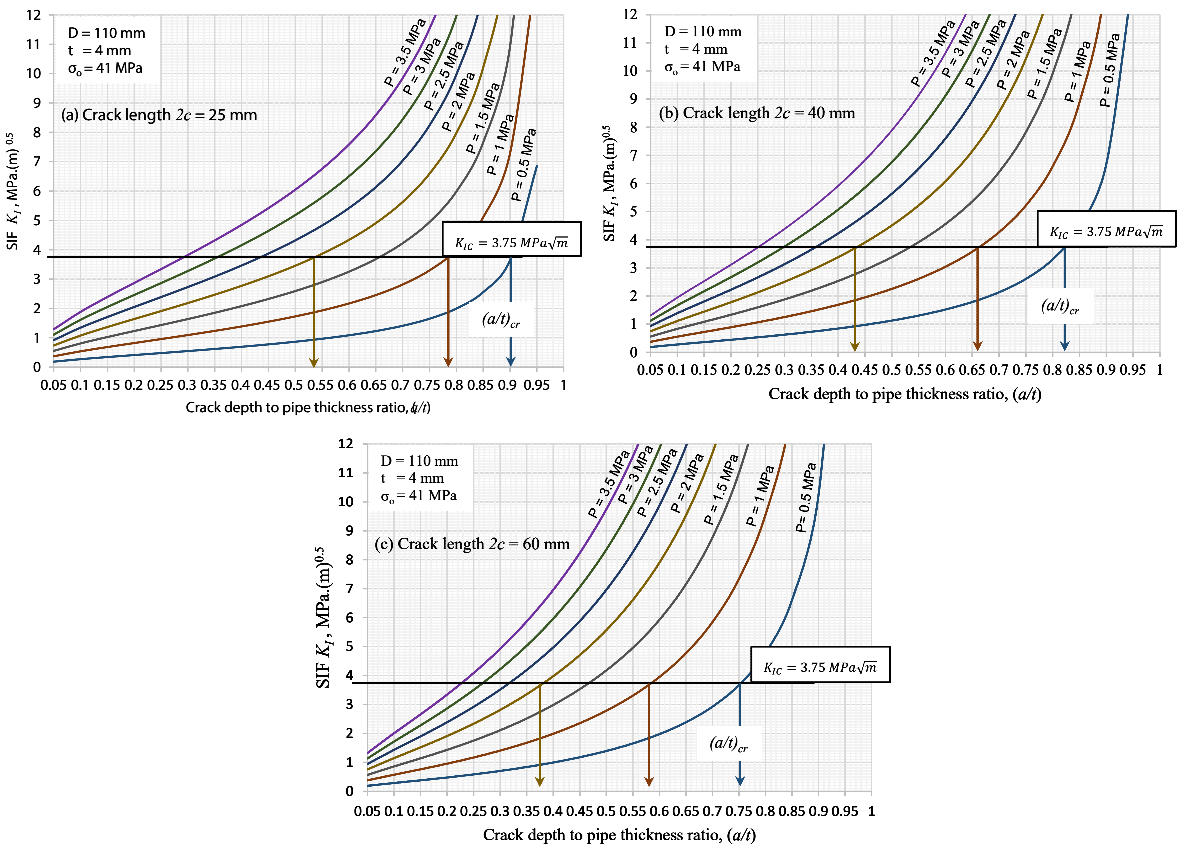

Fig. 14. Variation of stress intensity factor SIF (K_I) with relative crack depth (a/t) for constant crack length (a) $2c = 25$ mm; (b) $2c = 40$ mm; (c) $2c = 60$ mm.

5.2. Theoretical results

The theoretical analysis is applied to obtain the values of SIF (K) as a function of the initial crack size by using the previously mentioned Eq. (1). Therefore, this analysis can be used to determine the critical crack size of cracked pipes by the critical value of SIF (K_{IC}).

5.2.1. Evaluation of critical crack depth

Fig. 14 shows the relation between the stress intensity factor and the crack depth to pipe thickness under various internal pressures for different crack lengths. From the figure, the critical value of crack depth is predicted by using the fracture toughness value of uPVC material. The material toughness is given as $K_{IC} = 3.75\ MPa\sqrt{m}$ according to the manufacturer's data sheet. The values of critical relative crack depth are obtained by drawing a straight line at $K = K_{IC}$ intersecting (K - a/t) curves of various pressures for each crack length. The pipe dimensions and material properties are shown in Fig. 14. The value of stress intensity factor varies with crack depth to pipe thickness ratio (a/t) at constant crack length $2c$ for different pressures. The critical relative crack depth $(a/t)_{cr}$ is predicted early with increasing the internal pressure. Fig. 14 a, shows that the critical crack depth to thickness ratios $(a/t)_{cr}$ are 0.902, 0.538 and 0.292 for internal pressures of 0.5, 2 and 3.5 MPa, respectively. Also, at internal pressure $P = 2$ MPa, the critical crack depth to thickness ratios $(a/t)_{cr}$ are found to be 0.538, 0.4365 and 0.3825 for the crack lengths $2c$ of 25, 40 and 60 mm, respectively. It is noticed that the value of the critical crack depth is significantly affected by the value of the internal pressure while the crack length is not affected in the same level.

5.2.2. Failure assessment diagrams

Fig. 15 shows the FAD of pipes with axial surface crack for different crack lengths. The FAD is applied for pipes of diameter 110 mm and thickness 4 mm under different pressures from 0 to 3.5 MPa for each crack length. The failure assessment line is plotted using Eq. (4). The loading lines have been plotted using Eqs. (2) and (3) knowing the applied SIF (K_{app}) from Eq. (1) and the applied stress σ_{app}. Calculating K_{app} necessitates the calculation of σ_{app} which is a function of the applied pressure. The loading lines are obtained by the relation between the toughness ratio K_r and the load ratio L_r for various a/t ratios. The toughness ratio K_r is calculated by dividing the applied SIF (K_{app}) by the fracture toughness for the material (K_{IC}). The load ratio L_r is calculated from the Eq. (3). The relationship between the two parameters K_r and L_r is expressed by the assessment points that increase by increasing the internal pressure until it reaches the failure assessment line, then failure occurs. The assessment points that are located below the failure assessment line are safe and the points are located out of it are unsafe. As provided by the equation (3), the load ratio depends on the hoop stress, yield strength, crack length and crack depth for the investigated axial crack condition. The results indicates an increase in the slope of the assessment points when the crack length increases for a fixed crack depths. However, the failure assessment line which is a function of load ratio (L_r) was observed to be overlapped over each other for different combinations of crack depths and crack lengths (Fig. 16). This evidently shows the failure assessment line in failure assessment diagram plotted using Eq. (3) and Eq. (4) mainly depends on the internal pressure and material property whereas the cracks have no significant effect on the failure assessment line. However, the change in the slope of the assessment points of the failure assessment diagram illustrates a clear influence of the crack depth and crack length that helps to evauate the condition of the pipe under the action of internal pressure in the presence of cracks.

5.3. Estimation of burst pressure

Fig. 17 presents the agreement between the experimental and the theoretical critical values of burst pressure for the considered crack depth to pipe thickness ratio of pipes. The theoretical values were calculated using two analytical methods such as SIF method and the FAD method. Each curve at a specified crack length is considered as a critical curve used for assessing the structural integrity for a given crack depth under a loading condition (a/t, P). The points that lie in the region above the curve indicate the unsafe pressure zone whereas the pressures below the curve are safe to operate. The theoretical SIF curve values for each crack length is obtained using Fig. 14 from the intersection points of the straight line $K = K_{IC}$ with (K - a/t) curves of various pressures. Likewise, the FAD theoretical curve values for each crack length are obtained using Fig. 15 from the intersection points of the failure assessment line $K_r = f(L_r)$ with loading lines for each crack size. The experimental curves are plotted assuming the coefficient of friction between the steel balls with pipe wall equals 0.3. It is observed that the burst pressure reduced with the increased critical crack depth to pipe thickness ratio for a fixed crack length. This reduction is comparatively higher for both theoretical SIF and FAD approaches for the range of $(a/t)_{cr}$ from 0.25 to 0.75, whereas the difference in the burst pressure from the experimentation is very minimal within this range. It is concluded that the burst pressure using the FAD approach is more converging to the experimental burst pressure compared to SIF part-through assessment method. A considerable difference in the range between $a/t = 0.25$ to 0.35 may be due to the resistance offered by the material to the burst pressure and plastic deformation. For this reason, SIF method is not appropriate in this case for evaluating the ductile materials. However, the burst pressures estimated from the stress intensity factor approach and failure assessment diagram are close to the experimental burst pressures at 0.5 critical crack depth to thickness ratio, $(a/t)_{cr}$. Here, burst pressure values converged significantly and the good agreement of SIF to the experimental results is anticipated due to the less resistance of the material and brittle failure at comparatively higher crack depth to thickness ratio. The maximum margin of difference is only 0.29 MPa and 0.4 MPa for SIF and FAD approach respectively at 0.5 $(a/t)_{cr}$. At 0.75 $(a/t)_{cr}$, the burst pressures estimated by the FAD and SIF are nearly the same, however, there is a deviation from the experimental burst pressure. This maximum deviation is 0.94 and 0.93 for the SIF and FAD approach compared to the experimental burst pressure. At higher $(a/t)_{cr}$, the maximum difference in the burst pressure values

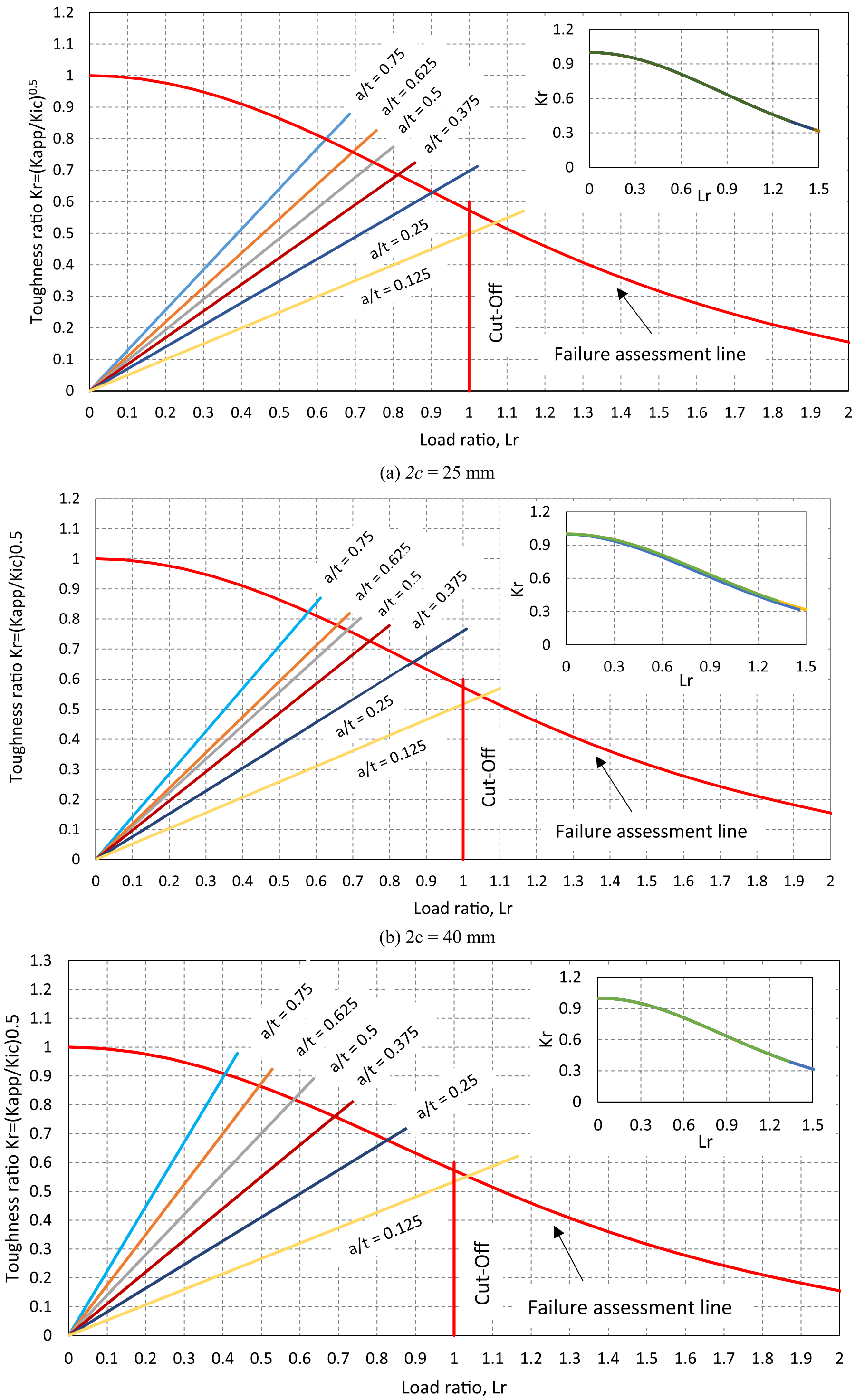

(a) $2c$ = 25 mm

(b) 2c = 40 mm

(c) 2c = 60 mm

Fig. 15. Failure assessment diagram for pipe made of uPVC containing an axial surface crack for different crack sizes at various pressure. (a) $2c = 25$ mm; (b) $2c = 40$ mm; (c) $2c = 60$ mm.

from the SIF and FAD approach is very minimal limited to 0.07 MPa. Therefore, the theoretical values were converging as the critical crack depth to pipe thickness increased. The study shows that the internal pressurization using bearing steel balls can be used in the absence of uniform hydrostatic pressurization for investigating the fracture phenomenon. However, a validation of the current

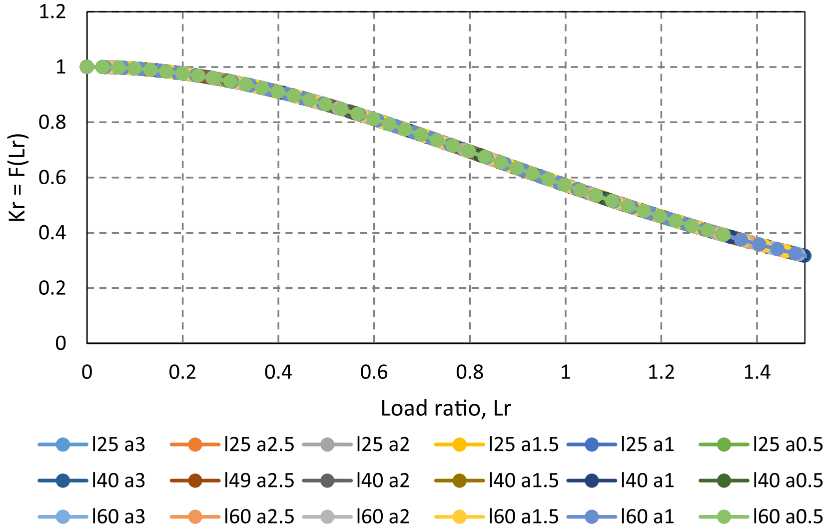

Fig. 16. Failure assessment line for pipe made of uPVC containing an axial surface crack for different crack depths and crack lengths. (l is crack length and a is crack depth).

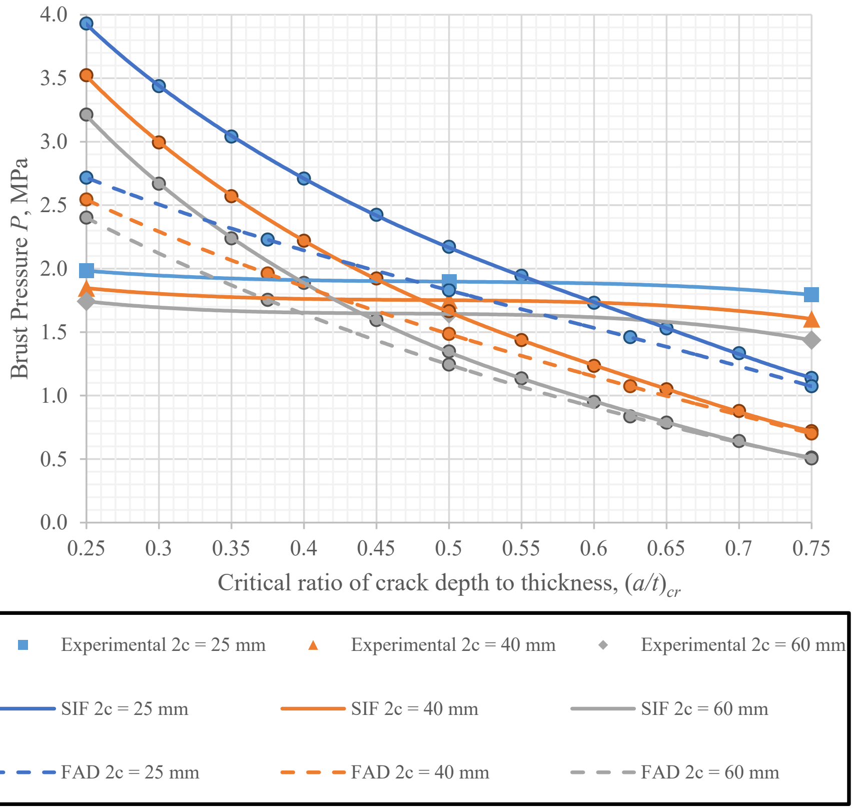

Fig. 17. Variation of the critical ratio of the crack depth to pipe thickness $(a/t)_{cr}$ with burst pressure P for certain crack length $2c$.

proposed approach with standard hydrostatic pressurization is highly recommended in future.

6. Conclusions

The study focused on introducing a novel approach by internally pressurizing the pipes with steel balls for experimentally evaluating the effect of crackles and cracked pipe joints. Two different analytical approaches such as the failure assessment diagram and stress intensity factor approach are compared with the experimental results. As a result of compressive force exerted on the steel balls in the pipes, cracks were formed in pipes due to maximum tensile stress or hoop stress along the longitudinal direction whereas, the crack propagated from the deepest point on the artificially cracked samples in the radial direction followed by in the longitudinal direction. The cracks and the severity of the cracks considerably reduced the burst pressure. Failure assessment diagram which is an elastic–plastic fracture mechanics parameter is more suitable over linear elastic fracture parameter, stress intensity factor approach for estimating the fracture behaviour. For the uPVC pipe, the deviation of burst pressures using SIF and FAD approach from the experimental evaluation is limited to the range between 0.07 and 0.94 MPa at ratio of crack depth to pipe thickness equals 0.5 and 0.75. Therefore, the results of the analytical analysis were found to be in good agreement with the experimental burst test for $(a/t)_{cr}$ in the range between 0.35 and 0.75. A significant difference of burst pressure between the SIF approach and experimental burst pressure in the range between $a/t = 0.25$ to 0.35 may be due to the resistance offered by the material to the burst pressure and plastic deformation indicating the inappropriateness of SIF approach for evaluating the ductile materials. From the theoretical evaluation of critical crack depth, it is noticed that the critical crack depth is significantly affected by the internal pressure while the effect of the crack length is less significant. Also, the failure assessment line in failure assessment diagram was found to be converged without any significant change for various combinations of crack depths and crack lengths. The study was found to be promising in the absence of hydrostatic internal pressurization technique. The future scope of the current investigation is to extend the experimentation using hydrostatic testing for comparing with the current technique.

CRediT authorship contribution statement

Mohamed El-Sayed: Investigation, Methodology, Resources, Writing – original draft, Visualization, Validation. **Aly El Domiaty:** Formal analysis, Investigation, Methodology, Resources, Supervision, Validation, Writing – original draft, Conceptualization. **Abdel-Hamid I. Mourad:** Conceptualization, Writing – original draft, Writing – review & editing, Visualization, Validation, Supervision, Project administration, Methodology, Investigation, Funding acquisition, Formal analysis. **Dinu Thomas Thekkuden:** Writing – review & editing, Resources.

Declaration of Competing Interest

The authors declare that they have no known competing financial interests or personal relationships that could have appeared to influence the work reported in this paper.

Acknowledgement

The authors would like to acknowledge UAE University for providing the facilities and funds through Materials library (#31N392) - Industry 4.0 district project.

References

[1] Mourad A-H, Alghafri MG, Abu Zeid OA. Stable crack extension through AISI 4340 steel: Experimental investigation, in. Key Eng Mater, Trans Tech Publ 2004; 261-263:207–12.
[2] Mourad AHI, Alghafri MJ, Abu Zeid OA, Maiti SK. Experimental investigation on ductile stable crack growth emanating from wire-cut notch in AISI 4340 steel. Nucl Eng Des 2005;235(6):637–47.
[3] Kawaguchi S, Hagiwara N, Masuda T, Toyoda M. Evaluation of leak-before-break (LBB) behavior for axially notched X65 and X80 line pipes. J Offshore Mech Arct Eng 2004;126:350–7.
[4] Kim Y-J. Non-linear fracture mechanics analysis of through-wall cracked pipes for leak-before-break analysis. J Press Equip Syst 2004;2:71–8.
[5] Kim Y-J, Huh N-S, Kim Y-J. Engineering J estimation methods for leak-before-break analyses of nuclear piping, JSME Int. J. Ser. A Solid Mech. Mater Eng 2005; 48(1):41–50.
[6] J. Sharples, STYLE: comparison of leak-before-break methodologies applied in europe, in: Press. Vessel. Pip. Conf., American Society of Mechanical Engineers, 2012: pp. 763–768.
[7] M. El-Sayed, A. El Domiaty, A.-H. I Mourad, M. Lotfy, Leak Before Break Fracture Assessment for X70 Steel Pressurized Tubes With Axial Surface Crack, in: ASME 2018 Press. Vessel. Pip. Conf., American Society of Mechanical Engineers Digital Collection, 2018.
[8] A.-H.I. Mourad, E. Elghandour, F.A. Kolkailah, Mixed mode stable crack extensions through stiffened specimens, (1999).
[9] Maiti SK, Kishore GK, Mourad A-H- I. Bilinear CTOD/CTOA scheme for characterisation of large range mode I and mixed mode stable crack growth through AISI 4340 steel. Nucl Eng Des 2008;238(12):3175–85.
[10] Maiti SK, Mourad A-H-I. Criterion for mixed mode stable crack growth-I. Three point bend geometry. Eng Fract Mech 1995;52(2):321–47. https://doi.org/10.1016/0013-7944(95)00026-R.
[11] Mourad A-H- I, Maiti SK. MODE I AND MIXED-MODE STABLE CRACK EXTENSIONS THROUGH STIFFENED THREE-POINT BEND SPECIMENS. Fatigue Fract Eng Mater Struct 1995;18(6):645–52.
[12] A.-H.I. Mourad, Effect of stress state on mode II stable crack extension, in: Key Eng. Mater., Trans Tech Publ, 2005: pp. 1604–1610.
[13] Mourad AHI, Maiti SK. Influence of state of stress on mode I and mixed mode stable crack growth through stiffened TPB specimens, Acta Mech. Solida Sin. Off J Chinese Soc Theor Appl Mech 1995;8:99–102.
[14] Maiti SK, Mourad A-H-I. Criterion for mixed mode stable crack growth—II. Compact tension geometry with and without stiffener. Eng Fract Mech 1995;52(2): 349–78.
[15] Mourad A-H- I, Maiti SK. Influence of state of stress on mixed mode stable crack growth through D16AT aluminium alloy. Int J Fract 1995;72(3):241–58.
[16] Mourad A-H-I, Maiti SK. Mode II stable crack growth. Fatigue Fract Eng Mater Struct 1996;19:75–84. https://doi.org/10.1111/j.1460-2695.1996.tb00933.x.
[17] Mourad AHI, Altarawneha J, Domiaty AE, Chao YJ, Haggag FM. Fracture Toughness Measurements From Circumferentially-Notched Pipes Tests. Mater Perform Charact 2014;3:305–21.

[18] A.H. Mourad, J. Altarawneh, A. El Domiaty, Y.J. Chao, Fracture toughness determined from full-scale pipe, in: ASME 2012 Press. Vessel. Pip. Conf., American Society of Mechanical Engineers Digital Collection, 2012: pp. 125–130.
[19] El-Sayed M, Domiaty AE, Mourad A-H-I. Fracture assessment of axial crack in steel pipe under internal pressure. Procedia Eng 2015;130:1273–87.
[20] Gajdoš Ľ, Šperl M. Application of a fracture-mechanics approach to gas pipelines. Int J Mech Mechatronics Eng 2011;5:67–74.
[21] A.-H. Mourad, J. Altarawneh, A. El Domiaty, Fracture Assessment of X65 Steel Pipe With Through-Wall Crack Under Pure Bending, in: ASME 2013 Press. Vessel. Pip. Conf., American Society of Mechanical Engineers Digital Collection, 2013.
[22] G. Pluvinage, Defect Assessment on Pipe Transporting a Mixture of Natural Gas and Hydrogen, in: Damage Fract. Mech., Springer, 2009: pp. 19–32.
[23] Milne I, Ainsworth RA, Dowling AR, Stewart AT. Assessment of the integrity of structures containing defects. Int J Press Vessel Pip 1988;32(1-4):3–104.
[24] Šarkoćević Ž, Arsić M, Sedmak A, Međo B, Mišić M. Assessment of the integrity of welded pipes. Zaštita Mater 2014;55(3):287–92.
[25] Sharma RK, Shrivastava SK, Dixit PM, Basu S. On the problem of an axial semi-elliptical crack in a hollow ductile cylinder. Int J Fract 2006;140(1-4):269–75.
[26] I. Skozrit, Z. Tonković, On numerical analysis of creep fracture behaviour of medium density polyethylene, in: Key Eng. Mater., Trans Tech Publ, 2010: pp. 233–236.
[27] Z. Tonkovic, I. Skozrit, J. Soric, A contribution to assessment of steam generator tubes integrity, in: 11th Int. Conf. Fract. Turin, Italy, 2005.
[28] M.A. Bouaziz, M.A. Guidara, M. Dallali, C. Schmitt, E.H. Taieb, Z. Azari, Collapse analysis of longitudinally cracked HDPE pipes, in: Int. Conf. Des. Model. Mech. Syst., Springer, 2017: pp. 559–568.
[29] Duvall DE, Edwards DB. Oxidative degradation of high density polyethylene pipes from exposure to drinking water disinfectants. ESI Report: File; 2009. p. 1–75.
[30] C. Devilliers, Dégradation chimique du PE et influence sur le comportement, l'endommagement et la rupture en fluage: application à la durabilité des canalisations sous pression, (2011).
[31] Guevara-Morales A, Leevers P. Experimental investigation of the effect of residual stresses and interfacial adhesion on rapid crack propagation in bilayered polypropylene/polyethylene (PP/PE 100) pipes. Polym Eng Sci 2017;57(4):458–63.
[32] Farshad M. Plastic pipe systems: Failure investigation and diagnosis. Elsevier; 2011.
[33] Dallali M, Guidara MA, Bouaziz MA, Schmitt C, Haj-Taieb E, Azari Z. Accuracy and security analysis of transient flows in relatively long pipelines. Eng Fail Anal 2015;51:69–82.
[34] Ahmed WK, Mourad AHI. Strengthening of Misaligned Welded Pipes with Outer Circumferentially Crack Using FRP Bandage Finite Element Analysis. J Mech Eng 2013;1:66–73.
[35] Guidara MA, Bouaziz MA, Schmitt C, Azari Z, Hadj-Taieb E. A semi-empirical model for structural integrity assessment of defected high density polyethylene pipes. Eng Fail Anal 2019;100:273–87.
[36] Ahmed WK, Mourad A-H- I. Fracture assessment of strengthened cracked metallic components using FRP stiffeners. Mech Compos Mater 2015;51(3):301–12.
[37] Guidara MA, Bouaziz MA, Schmitt C, Capelle J, Taïeb EH, Azari Z, et al. Structural integrity assessment of defected high density poly-ethylene pipe: Burst test and finite element analysis based on J-integral criterion. Eng Fail Anal 2015;57:282–95.
[38] Guidara MA, Bouaziz MA, Dallali M, Schmitt C, Taieb EH, Azari Z. HDPE pipe failure analysis under overpressure in presence of defect, in. Int Conf Des Model Mech Syst, Springer 2017:1027–38.
[39] M.F. Ghazali, G. Priyandoko, W.S.W. Hamat, T.W. Ching, Plastic pipe crack detection using ultrasonic guided wave method, in: Proc. Malaysian Tech. Univ. Conf. Eng. Technol. Melaka, Malaysia, 2014: pp. 10–11.
[40] Zhu J, Collins RP, Boxall JB, Mills RS, Dwyer-joyce R. Non-destructive in-situ condition assessment of plastic pipe using ultrasound. Procedia Eng 2015;119: 148–57.
[41] Rodolfo Jr A. Application of fracture mechanics for the characterization of PVC pipes. I. Evaluation of the applicability of the EWF technique in specimens produced directly from pipes. J Vinyl Addit Technol 2021;27:240–53.
[42] Yang J, Hu S. Estimation of Burst Pressure of PVC Pipe Using Average Shear Stress Yield Criterion: Experimental and Numerical Studies. Appl Sci 2021;11: 10477.
[43] S. Folkman, Validation of the long life of PVC pipes, in: Proc. 17th Int. Conf. Plast. Pipes, Chicago, USA, 2014.
[44] J.M. Greig, T.R. Smith, Plastic Gas Pipes-Fracture Considerations, in: Plast. Inst. Conf. Des. to Avoid Mech. Fail. Cranf. Inst. Tech., Pap., 1973.
[45] Darwish AY, Mandell JF, Mcgarry FJ. Applicability of linear elastic fracture mechanics to rigid PVC pipe materials. J Vinyl Technol 1981;3(4):246–50.
[46] Jamarani MB, Reed PE, Davies WR. Fracture behaviour of UPVC thin tubes at high loading rates. J Mater Sci 1988;23(12):4437–44.
[47] C.F. Tiffany, J.N. Masters, Applied fracture mechanics, in: Fract. Toughness Test. Its Appl., ASTM International, 1965.
[48] Shah RC, Kobayashi AS. Stress intensity factors for an elliptical crack approaching the surface of a semi-infinite solid. Int J Fract 1973;9(2):133–46.
[49] Scott PM, Thorpe TW. A critical review of crack tip stress intensity factors for semi-elliptic cracks. Fatigue Fract Eng Mater Struct 1981;4(4):291–309.
[50] Newman JC. Fracture analysis of surface-and through-cracked sheets and plates. Eng Fract Mech 1973;5(3):667–89.
[51] F.W. Brust, P. Scott, S. Rahman, Assessment of short through-wall circumferential cracks in pipes. Experiments and analysis: March 1990–December 1994, Nuclear Regulatory Commission, 1995.
[52] Milne I, Ainsworth RA, Dowling AR, Stewart AT. Background to and validation of CEGB report R/H/R6—Revision 3. Int J Press Vessel Pip 1988;32(1-4):105–96.
[53] Mourad A-H, El-Domiaty A, Chao YJ. Fracture toughness prediction of low alloy steel as a function of specimen notch root radius and size constraints. Eng Fract Mech 2013;103:79–93.
[54] Mourad AHI, Abu-Assi A, Haggag FM, Chao YJ. Novel Technique for Normalizing Load-Displacement Curves in Fracture Testing. Mater Perform Charact 2014;3: 1–20.
[55] Al Laham S, Branch SI. Stress intensity factor and limit load handbook. British Energy Generation Limited Gloucester, UK 1998.
[56] I.s.o.. 6259–3, Thermoplastics Pipes—Determination of Tensile Properties—Part 3. Polyolefin Pipes 1997.
[57] Long WM. Radial pressures in powder compaction. Powder Metall 1960;3(6):73–86.
[58] A. Hogänäs, Compacting of Metal Powders, PM Sch. Handb. 2 (n.d.).
[59] Roman OV. Theory and practice of metal powder molding processes. Sov Powder Metall Met Ceram 1967;6(10):783–9.
[60] Agarwal PK, Sinha SK. Elements of physics XI. Rastogi Publications 2008.
[61] Coefficient of friction for a range of material combinations, (n.d.). https://www.tribology-abc.com/abc/cof.htm (accessed November 7, 2021).